

A global potential constrained by the Bohr-Sommerfeld quantization condition for α -decay half-lives of even-even nuclei

Nguyen Gia Huy^a, Do Huy Tho^a, Mai Doan Quang Huy^a, Nguyen Le Anh^{a,*}

^aDepartment of Physics, Ho Chi Minh City University of Education, 280 An Duong Vuong, Cho Quan Ward, Ho Chi Minh, Vietnam

Abstract

The α decay provides valuable constraints on nuclear structure and plays an essential role in identifying heavy and superheavy nuclei. We study α -decay half-lives of 178 even-even nuclei within a semi-classical WKB framework using a phenomenological Woods-Saxon α -nucleus potential. The potential depth is determined by imposing the Bohr-Sommerfeld quantization condition (BSQC), ensuring a physically consistent description of the quasibound α -daughter system. To facilitate large-scale calculations, a global parametrization of the BSQC-constrained potential depth is constructed. The resulting half-lives reproduce experimental data with comparable accuracy for both the direct BSQC approach and the fitted prescription, providing a first step toward a global and computationally efficient description of α decay.

Keywords: alpha decay, half-life, WKB, Bohr-Sommerfeld quantization condition

1. Introduction

Alpha (α) decay is one of the dominant decay modes of heavy and superheavy nuclei, representing a paradigmatic example of quantum tunneling that historically served as an early test of the Schrödinger equation. Owing to its clean experimental signature, α decay provides precise information on ground-state energies, lifetimes, and spin-parity assignments, and it remains a primary tool for the identification of new isotopes and elements [1, 2]. With more than 400 known α emitters and continued advances in radioactive-beam production and detection techniques, α decay continues to offer a sensitive probe of nuclear structure, including clustering phenomena, shell effects, effective interactions, and nuclear deformation [3–9].

A wide variety of theoretical approaches have been developed to describe the α -decay process [10], ranging from fully microscopic models based on mean-field or energy-density-functional theories to macroscopic fission-like descriptions [11]. In addition to these approaches, the cluster model framework offers a particularly transparent physical picture. In this framework, the parent nucleus is assumed to preform an α particle composed of four valence nucleons, which subsequently moves in the mean-field potential generated by the daughter nucleus [8]. The decay is then described as quantum tunneling of the α particle through the combined nuclear and Coulomb barrier, following the seminal interpretations of Gamow [12] and of Gurney and Condon [13, 14]. The penetration probability is commonly evaluated using the Wentzel-Kramers-Brillouin (WKB) semi-classical approximation [15–17].

Within the WKB framework, the α -nucleus interaction potential is a central ingredient, as it governs both the quasibound internal motion and the barrier penetrability. Microscopic α -nucleus potentials constructed using folding models with realistic density-dependent nucleon-nucleon (NN) interactions have been shown to provide a consistent description of elastic scattering, bound-state properties, and α decay [16, 18–20]. Owing to the dominance of the real part of the interaction, α decay offers a particularly suitable testing ground for reducing the number of free parameters in the α -nucleus potential. In particular, Ref. [16] demonstrated that a proper implementation of the Bohr-Sommerfeld quantization condition (BSQC) within such microscopic potentials imposes stringent constraints on the α -nucleus interaction and significantly improves the agreement between calculated and experimental α -decay half-lives. These studies underline the predictive capability of microscopic potentials when both surface and interior regions of the interaction are reliably described.

Despite these successes, microscopic folding potentials require detailed nuclear density distributions and effective NN interactions, which can limit flexibility and increase computational cost in large-scale or systematic studies. For this reason, phenomenological α -nucleus potentials remain widely used [21, 22]. It is noted that both double-folding (DF) potentials and phenomenological Woods-Saxon (WS) potentials have been extensively applied as effective interactions in the analysis of nuclear reactions, scattering, and decay phenomena. When constrained by physically motivated conditions, such as reproducing the experimental Q_α value through the BSQC, phenomenological potentials can provide a reliable and efficient description of the quasibound α -daughter system while retaining sensitivity to essential nuclear structure effects. However, the practical application of BSQC-constrained potentials in large-

*Corresponding author

Email address: anhn1@hcmue.edu.vn (Nguyen Le Anh)

scale surveys is hindered by the need to solve semi-classical quantization conditions individually for each nucleus.

In the present work, α decay is investigated within the semi-classical WKB framework using a phenomenological WS α -nucleus potential combined with the BSQC. While the BSQC provides an essential physical constraint and improves the reliability of α -decay calculations, its direct implementation requires iterative solutions of transcendental integrals for each nucleus, rendering large-scale applications computationally demanding. To address this limitation, the WS potential depths determined from the BSQC are used to construct a fitted parametrization following the functional form proposed in Ref. [23]. Unlike approaches that directly extract the potential depth from experimental half-lives, the present work determines the WS potential depth from the quasibound-state condition imposed by the BSQC, ensuring physical consistency at the wave-function level. This strategy aims to enhance numerical efficiency and consistency while reducing the complexity associated with repeated integral evaluations. The resulting α -decay half-lives are then compared with those obtained from direct BSQC-based calculations and alternative depth-determination methods to assess the accuracy and reliability of the proposed approach. The present study is therefore intended as a first step toward a global and computationally efficient description of α decay based on phenomenological potentials constrained by semi-classical quantization.

The present study is restricted to 178 even-even nuclei, for which α decay predominantly proceeds between the ground states of the parent and daughter nuclei. Transitions to excited states of the daughter nucleus are strongly hindered and contribute negligibly to the total decay width in systematic half-life calculations [3, 24]. Consequently, all α decays considered in this work are treated as ground-state to ground-state transitions and are calculated with orbital angular momentum $L = 0$.

The remainder of this paper is organized as follows. Section 2 describes the theoretical framework and computational methods, including the phenomenological potential model employed in this work, as well as the WKB approximation and the implementation of the BSQC. The calculated α -decay results obtained using the WS potential with depths determined from both the BSQC and the proposed fitted prescription are presented and discussed in Section 3. Finally, the main conclusions are summarized in Section 4.

2. Theoretical framework and method of calculation

2.1. Semi-classical description for α decay

The α -decay half-life $T_{1/2}$ of a nucleus is expressed as

$$T_{1/2} = \frac{\ln 2}{\lambda}, \quad (1)$$

where λ is the total α -decay constant.

In the α cluster model, the decay constant λ is written as the product of three factors [5, 25],

$$\lambda = S_\alpha \nu P, \quad (2)$$

where S_α is the α -particle preformation or spectroscopic factor, ν is the assault frequency, and P is the barrier penetration probability evaluated within the WKB approximation.

In the cluster model, the α particle is assumed to be preformed inside the parent nucleus and to move relative to a rigid daughter core. The preformation factor S_α accounts for the probability of α -nucleus formation prior to tunneling. In the present work, S_α is evaluated using the analytical parametrization proposed in Ref. [4],

$$\log S_\alpha = a + b \left(A_d^{1/6} + A_\alpha^{1/6} \right) + c \frac{N}{\sqrt{Q_\alpha}} + d \sqrt{L(L+1)} + h, \quad (3)$$

where A_d and A_α are the mass numbers of the daughter nucleus and the α particle, respectively, N is the neutron number of the parent nucleus, Q_α is the α -decay energy, and L is the orbital angular momentum carried by the emitted α particle, as determined by spin-parity conservation. The coefficients a, b, c, d , and h are obtained from global fits to experimental α -decay data. Their numerical values, parameterized according to two neutron-number regions of the parent nucleus, are listed in Table 1.

Within the semi-classical description, the assault frequency ν characterizes the oscillatory motion of the preformed α particle between the inner classical turning points and is given by [15]

$$\nu = \frac{\hbar}{2\mu} \left[\int_{r_1}^{r_2} \left(\frac{2\mu}{\hbar^2} [Q_\alpha - V(r)] \right)^{-1/2} dr \right]^{-1}, \quad (4)$$

where μ is the reduced mass of the α -daughter system and $V(r)$ denotes the total interaction potential.

At each encounter with the barrier, the α particle has a finite probability to tunnel through and escape from the nucleus. Within the WKB approximation, the barrier penetration probability P is expressed as [24]

$$P = \exp \left[-2 \int_{r_2}^{r_3} \sqrt{\frac{2\mu}{\hbar^2} [V(r) - Q_\alpha]} dr \right]. \quad (5)$$

The quantities r_1 , r_2 , and r_3 in Eqs. (4) and (5) are the classical turning points defined by the condition $V(r) = Q_\alpha$, where Q_α is the α -decay energy taken from Ref. [26]. In practice, the inner turning point r_1 is very small, while the outer turning point r_3 can be determined approximately. Since the nuclear potential $V_N(r)$ rapidly vanishes at large distances, r_3 is obtained by solving the equation involving only the centrifugal and Coulomb components, $V_L(r) + V_C(r) = Q_\alpha$.

2.2. Bohr-Sommerfeld quantization condition

In the semi-classical description of α decay, the nuclear potential $V(r)$ must be capable of supporting a quasibound state

Table 1: Coefficients of Eq. (3) for the α -preformation factor, parameterized according to two neutron-number regions of the parent nucleus [4].

Region	a	b	c	d	h
$N \leq 126$	21.232	-6.210	0.003	-0.049	0
$N > 126$	37.421	-10.900	0.040	-0.088	0

of the α -daughter system prior to tunneling. This requirement is fulfilled by imposing the BSQC [20, 27],

$$\int_{r_1}^{r_2} \sqrt{\frac{2\mu}{\hbar^2} [Q_\alpha - V(r)]} dr = (2n + 1) \frac{\pi}{2}, \quad (6)$$

where $n = 0, 1, 2, \dots$ are the number of nodes of the quasibound radial wave function inside the potential well. It is related to the global quantum number G , which characterizes the relative motion of the α cluster and is determined by the Wildermuth-Tang rule [28],

$$G = 2n + L = \sum_{i=1}^4 (2n_i + \ell_i) = \sum_{i=1}^4 g_i, \quad (7)$$

where L is the orbital angular momentum carried by the emitted α particle, and n_i and ℓ_i are the radial and orbital quantum numbers of the four nucleons forming the α cluster. The values of g_i are chosen to enforce the Pauli exclusion principle by restricting the α -nucleus nucleons to orbitals above the occupied shells of the daughter nucleus. In the present work, $g_i = 4$ for nucleons in the shell $50 \leq N_d, Z_d \leq 82$, $g_i = 5$ for $82 < N_d, Z_d \leq 126$, and $g_i = 6$ for nucleons outside the $N_d = 126$ shell [16]. Additionally, we restrict the present analysis to the three regions $G = 18, 20$, and 22 , which mainly correspond to medium-heavy and heavy even-even nuclei where the α -cluster picture and the BSQC-based description are expected to be most reliable [23]. Under this restriction, 178 even-even nuclei are included in the systematic study, following Ref. [23]. For phenomenological potentials without an explicit repulsive core, the combined use of the BSQC and the Wildermuth-Tang prescription provides an effective implementation of Pauli exclusion effects, as discussed in Ref. [16].

The BSQC thus provides a physically motivated constraint on the nuclear potential, ensuring the correct oscillatory behavior of the quasibound wave function inside the potential well and reducing ambiguities in the choice of potential depth. Its implementation is therefore essential for obtaining reliable and consistent α -decay half-life calculations within the semi-classical framework.

2.3. Phenomenological α -nucleus potential

In α decay, only the real part of the α -nucleus interaction potential is relevant. Accordingly, the interaction potential employed in the present calculations consists of the nuclear, centrifugal, and Coulomb components

$$V(r) = V_N(r) + V_L(r) + V_C(r), \quad (8)$$

where the nuclear part $V_N(r)$ is described by a phenomenological Woods-Saxon (WS) potential,

$$V_N(r) = -V_0 \left[1 + \exp\left(\frac{r - R_0}{a_0}\right) \right]^{-1}, \quad (9)$$

where V_0 is the potential depth, R_0 is the nuclear radius of the daughter nucleus A_d , and a_0 is the diffuseness parameter. In this work, the depth V_0 is determined by imposing the BSQC

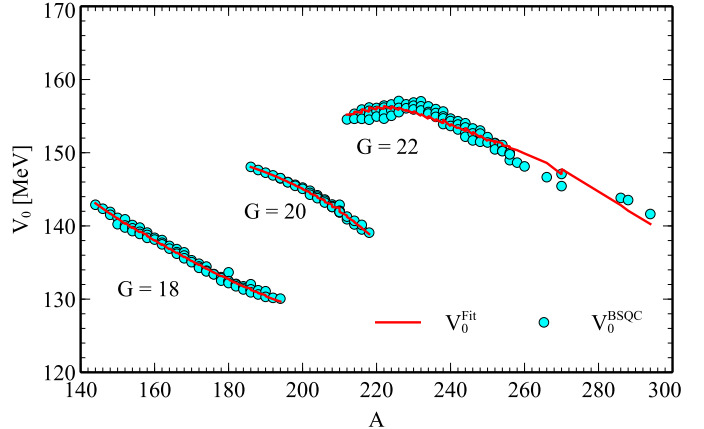


Figure 1: Depth V_0 of the WS potential determined from the BSQC for 178 even-even nuclei. These values are used to construct the fitted parametrization given in Eq. (12).

given in Eq. (6). The centrifugal potential $V_L(r)$ accounts for the orbital angular momentum carried by the emitted α particle and is given by

$$V_L(r) = \frac{\hbar^2}{2\mu r^2} \left(L + \frac{1}{2} \right)^2, \quad (10)$$

where the replacement of $L(L+1)$ by $(L+1/2)^2$ corresponds to the Langer modification [29], which ensures the correct behavior of the radial wave function near the origin and improves the validity of the WKB connection formulas [30].

The Coulomb interaction $V_C(r)$ between the daughter nucleus and the α particle is modeled by assuming a uniformly charged sphere,

$$V_C(r) = \begin{cases} \frac{Z_d e^2}{R_0} \left(3 - \frac{r^2}{R_0^2} \right), & r < R_0, \\ \frac{2Z_d e^2}{r}, & r \geq R_0, \end{cases} \quad (11)$$

where Z_d is the charge of the daughter nucleus. The radius parameter is taken as $R_0 = r_0 A_d^{1/3}$ with $r_0 = 1.27$ fm, and the diffuseness is fixed at $a = 0.64$ fm. These values correspond to the optimal parameters obtained by simultaneously varying r_0 and a_0 to minimize the rms deviation χ for the 178 even-even nuclei considered in this study. The sensitivity of the calculated results to these parameters and the optimized values are discussed in detail in Section 3.

3. Results and discussion

3.1. Bohr-Sommerfeld quantization condition-constrained Woods-Saxon potential depth

Figure 1 displays the depth V_0 of the WS potential obtained by imposing the BSQC. The results exhibit a clear separation into three distinct regions, corresponding to the three values of the global quantum number $G = 18, 20$, and 22 for the 178 nuclei considered. Overall, the potential depth shows a gradual decrease with increasing mass number A .

To improve computational efficiency and facilitate large-scale calculations, a fitted parametrization for the potential depth V_0 is introduced, following a functional form similar to that proposed in Ref. [23],

$$V_0^{\text{Fit}} = c_0 + \left(c_1 A^2 + c_2 A + c_3 E_{\text{sh}} \right) \frac{AZ}{Q_\alpha} \frac{1}{G}, \quad (12)$$

where A and Z are the mass and proton numbers of the parent nucleus, respectively. The quantity E_{sh} denotes the shell-correction energy of the parent nucleus, defined as the difference between the experimental binding energy and the macroscopic binding energy. The values of E_{sh} are taken from column 3 of Table I in Ref. [23]. Using the potential depths V_0 obtained from the BSQC, a least-squares fit is performed, and the resulting fitting coefficients are listed in Table 2.

The α -decay half-lives calculated using the potential depth V_0 determined directly from the BSQC are compared with those obtained using the fitted parametrization in Eq. (12). This comparison allows for an assessment of the accuracy and reliability of the fitted approach.

3.2. Calculated α -decay half-lives

To assess the accuracy of the two approaches used to determine the potential depth V_0 , the root-mean-square (rms) deviation χ of the decimal logarithm of the calculated half-lives with respect to experimental data is evaluated as [16]

$$\chi = \sqrt{\frac{1}{n-1} \sum_{i=1}^n \left(\log T_{1/2,i}^{\text{Cal}} - \log T_{1/2,i}^{\text{Exp}} \right)^2}, \quad (13)$$

where n is the total number of nuclei considered.

Figure 2 compares the logarithmic deviations $\log(T_{1/2}^{\text{Cal}}/T_{1/2}^{\text{Exp}})$ obtained using the two prescriptions for determining the potential depth V_0 . The results show that the calculated half-lives obtained with the fitted depth in Eq. (12) closely reproduce those obtained from the direct BSQC-based determination over the entire mass range $144 \leq A \leq 294$.

Quantitatively, the rms deviation for the BSQC-based calculation is $\chi_{\text{BSQC}} = 0.253$, demonstrating that the WS potential constrained by the BSQC provides a reliable description of α -decay half-lives. When the fitted parametrization in Eq. (12) is employed, a comparable deviation of $\chi_{\text{Fit}} = 0.250$ is obtained. The negligible difference between the two values indicates that the fitted prescription preserves the accuracy of the BSQC-based approach. A regional comparison of the rms deviations for nuclei grouped by the global quantum number G

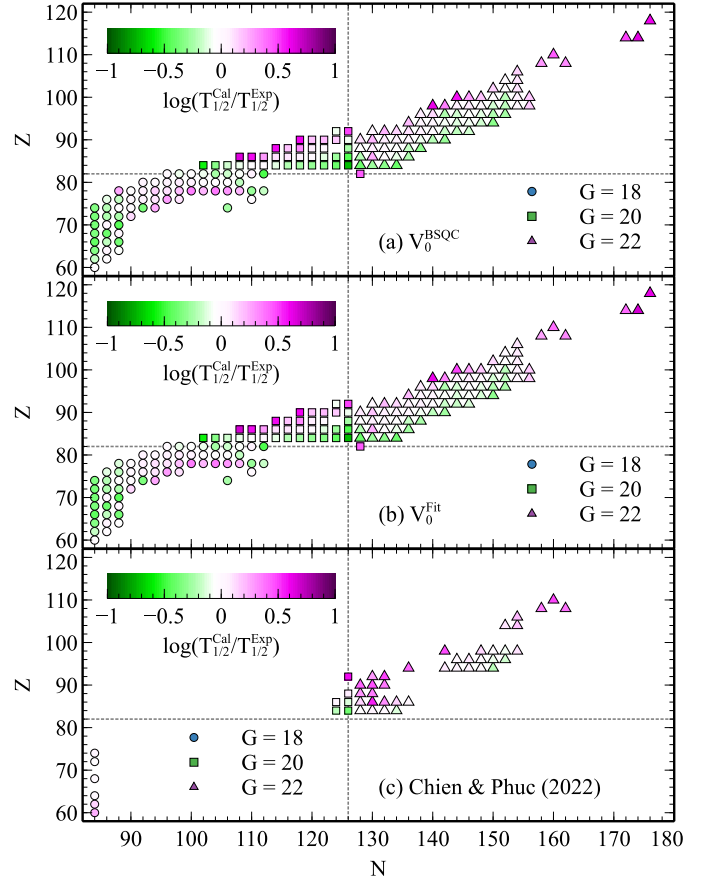


Figure 2: Nuclide-chart distribution of the decimal logarithmic deviation $\log(T_{1/2}^{\text{Cal}}/T_{1/2}^{\text{Exp}})$ between calculated and experimental α -decay half-lives, plotted as a function of the neutron and proton numbers (N, Z) of the parent nuclei. The color scale indicates the magnitude of the deviation. The results are obtained using the WS potential depth V_0 determined from the BSQC in Eq. (6) (a) and from the fitted parametrization in Eq. (12) (b). For comparison, results calculated with the semi-microscopic DF potential based on the CDM3Y3 interaction from Ref. [16] are shown in (c). The dotted lines indicate the magic numbers $N = 126$ and $Z = 82$. Experimental data are taken from Ref. [31].

is presented in Table 3. In all regions, the fitted parametrization yields deviations that are comparable to, or slightly smaller than, those obtained from the direct BSQC determination.

Notably, the most pronounced improvement is observed in the $G = 22$ region, where the potential depths obtained directly from the BSQC exhibit anomalous behavior, as shown in Figure 1. In this region, the fitted parametrization provides a smoother and more stable description of V_0 , leading to a clear reduction of the rms deviation from $\chi_{\text{BSQC}} = 0.237$ to $\chi_{\text{Fit}} = 0.226$. This behavior highlights the effectiveness of the fitted prescription in mitigating local irregularities inherent in the direct BSQC-based determination.

The agreement between calculated and experimental half-lives is more challenging for nuclei with $G = 20$ than for those with $G = 18$ and $G = 22$. This behavior reflects enhanced nuclear-structure effects in the $G = 20$ region. The α decay depends not only on barrier penetrability but also on the preformation factor S_α , which is known to exhibit significant fluctuations in transitional regions between major shell closures [32, 33].

Table 2: Fitting coefficients of the WS potential depth V_0 obtained using the parametrization in Eq. (12). All coefficients are given in MeV.

Region	c_0	c_1	c_2	c_3
$G = 18$	214.75	0.02	-12.04	0.0004
$G = 20$	47.45	-0.08	22.94	0.0002
$G = 22$	87.97	-0.04	15.53	-0.0025

Many $G = 20$ nuclei lie in regions of shape transition and moderate deformation, where shell effects and collective correlations compete. In this regime, the nuclear structure is dominated more strongly by mean-field configurations than by well-developed α -cluster correlations. Consequently, the α -cluster preformation becomes more sensitive to local shell structure and deformation effects, so that a single parametrization of the WS potential depth cannot fully capture local structural variations, leading to larger rms deviations.

For comparison, calculations performed using a semi-microscopic DF potential based on the CDM3Y3 NN interaction for 50 nuclei in Ref. [16] yielded an rms deviation of $\chi_{\text{DF}} = 0.259$, which is close to the present value being $\chi_{\text{Fit}} = 0.269$. It should be noted that in the present work, a single diffuseness parameter a_0 is adopted for all 178 nuclei, whereas an optimization of a_0 restricted to the subset of 50 nuclei could further reduce the deviation. The comparable rms deviations obtained with the WS and DF approaches demonstrate that the phenomenological WS potential provides a reasonable and competitive description of α decay.

From a practical perspective, the fitted potential-depth parametrization significantly reduces computational effort by avoiding repeated solutions of the BSQC integrals for each nucleus, while maintaining consistency and reliability in large-scale α -decay calculations. Detailed numerical values for all 178 nuclei are listed in Table 4.

3.3. Sensitivity to diffuseness and radius parameters

In addition to the pronounced dependence on the global quantum number G , the WS potential depth V_0 exhibits sensitivity to the geometrical parameters of the nuclear potential, namely the diffuseness a_0 and the radius parameter r_0 . To quantify this effect, the rms deviation χ was evaluated for diffuseness values in the range from 0.4 fm to 0.8 fm, while keeping r_0 fixed at 1.27 fm.

Figure 3 shows the variation of the rms deviation χ as a function of a_0 for the full set of 178 nuclei. Although the dependence is not strictly monotonic, a clear minimum is observed within the investigated range, indicating the existence of an optimal diffuseness value for systematic α -decay calculations. The optimal values of a_0 are found to be 0.63 fm, 0.65 fm, and 0.64 fm for the regions with $G = 18$, 20, and 22, respectively. The average optimal value over all regions is therefore $a_0 = 0.64$ fm. When the analysis is restricted to the 50 nuclei considered, Ref. [16], the optimized diffuseness

Table 3: The rms deviation χ of the calculated α -decay half-lives $T_{1/2}$ obtained using the WS potential depth V_0 determined from the fitted parametrization in Eq. (12) and from the BSQC in Eq. (6). Results are grouped according to the global quantum number G . The second column lists the number of nuclei in each region.

Region	n	χ_{Fit}	χ_{BSQC}
$G = 18$	65	0.216	0.218
$G = 20$	37	0.341	0.339
$G = 22$	76	0.226	0.237
Total	178	0.250	0.253

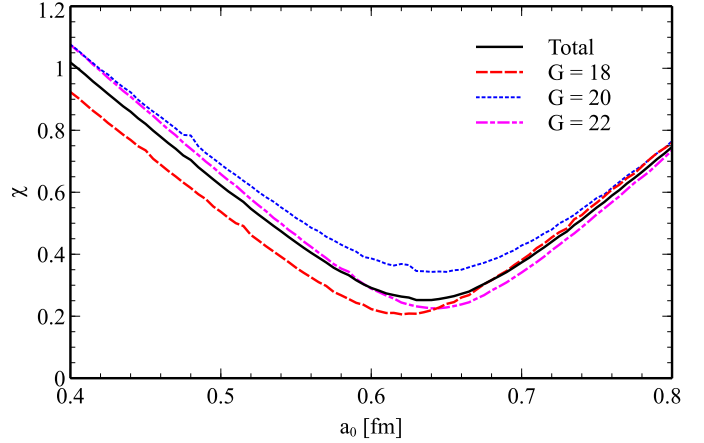


Figure 3: The rms deviation χ between the decimal logarithms of calculated and experimental α -decay half-lives as a function of the diffuseness parameter a_0 . The radius parameter is fixed at $r_0 = 1.27$ fm.

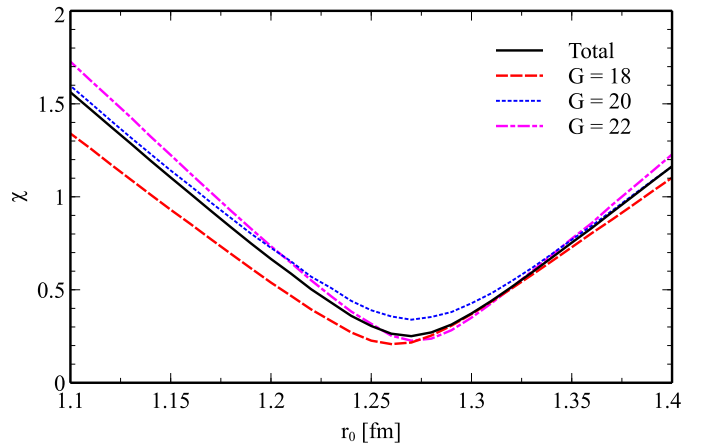


Figure 4: Same as Figure 3 but for the function of the radius parameter r_0 . The diffuseness parameter is fixed at $a_0 = 0.64$ fm.

Table 4: Parameters and calculated α -decay half-lives (in seconds). All calculations use $a_0 = 0.64$ fm and $r_0 = 1.27$ fm. The columns list: (2) the global quantum number G ; (3-4) the shell-correction energy E_{sh} [23] and the α -decay energy Q_α [26]; (5-6) the WS potential depth V_0 determined from the BSQC and from the fitted parametrization, respectively; (7-9) the calculated $\log T_{1/2}$ values obtained with these two prescriptions, and the corresponding experimental data [31].

α emitter	G	E_{sh} [MeV]	Q_α [MeV]	V_0^{BSQC} [MeV]	V_0^{Fit} [MeV]	$\log T_{1/2}^{\text{BSQC}}$	$\log T_{1/2}^{\text{Fit}}$	$\log T_{1/2}^{\text{Exp}}$
^{144}Nd	18	1.715	1.901	142.89	143.10	22.824	22.822	22.859
^{146}Sm	18	1.125	2.529	142.35	142.37	15.157	15.156	15.332
^{148}Sm	18	-0.049	1.987	141.91	141.65	23.248	23.256	23.299
^{148}Gd	18	0.857	3.271	141.52	141.70	9.016	9.014	9.350
^{150}Gd	18	-0.403	2.807	141.10	140.99	13.528	13.529	13.500
^{152}Dy	18	0.611	4.351	140.23	141.05	2.688	2.678	3.107
^{152}Gd	18	-1.349	2.204	140.90	140.28	21.461	21.469	21.533
^{152}Dy	18	-0.575	3.727	140.06	140.37	6.745	6.741	6.933
^{152}Er	18	0.710	4.934	139.79	140.43	0.704	0.696	1.057
^{154}Dy	18	-1.418	2.945	140.12	139.68	13.597	13.603	13.976
^{154}Er	18	-0.416	4.280	139.67	139.76	4.282	4.281	4.678
^{154}Yb	18	1.140	5.474	139.29	139.83	-0.724	-0.731	-0.355
^{156}Er	18	-1.141	3.481	139.77	139.11	9.999	10.008	9.989
^{156}Yb	18	0.041	4.810	139.20	139.18	2.432	2.432	2.417
^{156}Hf	18	2.116	6.026	138.91	139.26	-1.994	-1.999	-1.627
^{158}Yb	18	3.109	4.170	139.09	138.75	6.184	6.189	6.630
^{158}Hf	18	-0.742	5.405	138.77	138.55	0.580	0.583	0.810
^{158}W	18	0.756	6.612	138.37	138.61	-3.185	-3.188	-2.845
^{160}Hf	18	-0.125	4.902	138.38	137.99	3.050	3.061	3.288
^{160}W	18	1.877	6.066	138.14	138.07	-1.206	-1.206	-0.991
^{162}Hf	18	-0.722	4.416	138.07	137.38	5.810	5.820	5.690
^{162}W	18	0.647	5.678	137.70	137.45	0.371	0.374	0.420
^{162}Os	18	2.732	6.768	137.48	137.52	-2.789	-2.799	-2.680
^{164}W	18	-1.107	5.278	137.27	136.81	2.187	2.194	2.220
^{164}Os	18	1.777	6.479	136.90	136.92	-1.844	-1.845	-1.660
^{166}W	18	-0.550	4.856	136.83	136.27	4.375	4.384	4.740
^{166}Os	18	0.638	6.143	136.42	136.32	-0.589	-0.588	-0.590
^{168}Pt	18	2.349	7.292	136.20	136.38	-3.285	-3.664	-3.530
^{168}W	18	-0.801	4.501	136.39	135.71	6.439	6.448	6.199
^{168}Os	18	-0.044	5.816	135.95	135.75	0.741	0.744	0.690
^{168}Pt	18	1.715	6.990	135.58	135.82	-2.736	-2.739	-2.690
^{170}Os	18	-0.488	5.537	135.31	135.19	1.983	1.985	1.890
^{170}Pt	18	0.623	6.707	135.05	135.24	-1.789	-1.791	-1.860
^{172}Os	18	-0.696	5.224	134.84	134.65	3.482	3.484	3.210
^{172}Pt	18	-0.067	6.463	134.47	134.68	-0.841	-0.885	-0.991
^{172}Hg	18	1.666	7.524	134.28	134.75	-3.596	-3.603	-3.636
^{174}Os	18	-0.664	4.871	134.45	134.13	5.362	5.366	5.260
^{174}Pt	18	-0.492	6.183	133.89	134.14	0.167	0.163	0.061
^{174}Hg	18	0.642	7.233	133.79	134.19	-2.707	-2.712	-2.699
^{176}Pt	18	-0.685	5.885	133.42	133.62	1.393	1.390	1.199
^{176}Hg	18	0.051	6.897	133.38	133.66	-1.599	-1.603	-1.650
^{178}Pt	18	-0.642	5.573	133.01	133.12	2.786	2.784	2.430
^{178}Hg	18	-0.316	6.577	132.86	133.14	-0.446	-0.450	-0.521
^{178}Pb	18	0.632	7.789	132.53	133.18	-3.610	-3.618	-3.600
^{180}W	18	1.034	2.515	133.66	132.77	25.441	25.454	25.700
^{180}Pt	18	-0.424	5.276	132.46	132.64	4.245	4.243	4.029
^{180}Hg	18	-0.470	6.258	132.45	132.64	0.775	0.772	0.730
^{180}Pb	18	0.179	7.419	132.19	132.67	-2.491	-2.498	-2.390
^{182}Pt	18	-0.149	4.951	132.08	132.18	5.985	5.983	5.620
^{182}Hg	18	-0.426	5.996	131.98	132.16	1.858	1.856	1.890
^{182}Pb	18	-0.089	7.066	131.75	132.18	-1.320	-1.329	-1.260

Table 4: (Continued)

α emitter	G	E_{sh} [MeV]	Q_α [MeV]	V_0^{BSQC} [MeV]	V_0^{Fit} [MeV]	$\log T_{1/2}^{\text{BSQC}}$	$\log T_{1/2}^{\text{Fit}}$	$\log T_{1/2}^{\text{Exp}}$
$^{184}_{78}\text{Pt}$	18	0.285	4.599	131.75	131.73	8.082	8.082	7.790
$^{184}_{80}\text{Hg}$	18	-0.171	5.660	131.53	131.70	3.381	3.377	3.439
$^{184}_{82}\text{Pb}$	18	-0.202	6.774	131.32	131.70	-0.309	-0.314	-0.213
$^{186}_{76}\text{Os}$	18	1.919	2.821	132.04	131.44	22.773	22.781	22.800
$^{186}_{78}\text{Pt}$	18	0.825	4.320	131.23	131.31	9.943	9.942	9.730
$^{186}_{80}\text{Hg}$	18	0.253	5.204	131.34	131.27	5.661	5.662	5.710
$^{186}_{82}\text{Pb}$	18	-0.134	6.471	130.93	131.24	0.827	0.823	1.079
$^{186}_{84}\text{Po}$	20	-0.733	8.501	148.07	148.05	-5.049	-5.049	-4.470
$^{188}_{78}\text{Pt}$	18	1.455	4.007	130.86	130.90	12.244	12.244	12.530
$^{188}_{80}\text{Hg}$	18	0.860	4.709	131.21	130.85	8.529	8.534	8.720
$^{188}_{82}\text{Pb}$	18	0.201	6.109	130.64	130.81	2.304	2.301	2.470
$^{188}_{84}\text{Po}$	20	-0.680	8.082	147.64	147.70	-3.899	-3.900	-3.570
$^{190}_{84}\text{Pt}$	18	2.322	3.269	131.08	130.56	18.999	19.006	19.179
$^{190}_{82}\text{Pb}$	18	0.746	5.698	130.31	130.40	4.177	4.175	4.250
$^{190}_{84}\text{Po}$	20	-0.482	7.693	147.27	147.32	-2.770	-2.771	-2.611
$^{192}_{82}\text{Pb}$	18	1.539	5.222	130.18	130.01	6.609	6.611	6.550
$^{192}_{84}\text{Po}$	20	-0.050	7.320	146.90	146.92	-1.592	-1.592	-1.489
$^{194}_{82}\text{Pb}$	18	2.565	4.738	130.07	129.67	9.465	9.471	9.940
$^{194}_{84}\text{Po}$	20	0.559	6.987	146.50	146.50	-0.459	-0.459	-0.410
$^{194}_{86}\text{Rn}$	20	-0.421	7.862	146.53	146.47	-2.460	-2.438	-3.108
$^{196}_{84}\text{Po}$	20	1.384	6.658	145.99	146.05	0.768	0.767	0.777
$^{196}_{86}\text{Rn}$	20	-0.001	7.617	145.96	146.01	-1.745	-1.745	-2.328
$^{198}_{84}\text{Po}$	20	2.469	6.310	145.62	145.58	2.150	2.151	2.267
$^{198}_{86}\text{Rn}$	20	0.579	7.349	145.48	145.52	-0.880	-0.881	-1.159
$^{200}_{84}\text{Po}$	20	3.662	5.982	145.24	145.10	3.572	3.574	3.794
$^{200}_{86}\text{Rn}$	20	1.440	7.043	145.07	145.01	0.177	0.178	0.072
$^{202}_{84}\text{Po}$	20	5.070	5.701	144.81	144.59	4.887	4.890	5.143
$^{202}_{86}\text{Rn}$	20	2.489	6.774	144.51	144.48	1.186	1.186	1.093
$^{202}_{88}\text{Ra}$	20	0.661	7.880	144.27	144.42	-1.799	-1.801	-2.387
$^{204}_{84}\text{Po}$	20	6.520	5.485	144.19	144.06	5.983	5.984	6.276
$^{204}_{86}\text{Rn}$	20	3.632	6.547	144.01	143.93	2.067	2.068	2.013
$^{204}_{88}\text{Ra}$	20	1.477	7.637	143.79	143.85	-1.038	-1.039	-1.222
$^{206}_{84}\text{Po}$	20	8.041	5.327	143.60	143.51	6.808	6.810	7.146
$^{206}_{86}\text{Rn}$	20	4.875	6.384	143.44	143.35	2.726	2.727	2.740
$^{206}_{88}\text{Ra}$	20	2.468	7.415	143.20	143.26	-0.295	-0.296	-0.620
$^{208}_{84}\text{Po}$	20	9.622	5.216	142.92	142.93	7.558	7.536	7.961
$^{208}_{86}\text{Rn}$	20	6.144	6.261	142.71	142.75	3.251	3.250	3.373
$^{208}_{88}\text{Ra}$	20	3.453	7.273	142.59	142.64	0.179	0.178	0.107
$^{208}_{90}\text{Th}$	20	1.540	8.202	142.59	142.57	-2.022	-2.022	-2.620
$^{210}_{82}\text{Pb}$	20	11.360	3.792	142.89	142.48	15.006	15.012	14.567
$^{210}_{84}\text{Po}$	20	10.982	5.408	141.84	142.29	6.349	6.344	7.079
$^{210}_{86}\text{Rn}$	20	7.450	6.159	142.08	142.11	3.682	3.682	3.954
$^{210}_{88}\text{Ra}$	20	4.545	7.151	141.99	141.99	0.599	0.599	0.602
$^{210}_{90}\text{Th}$	20	2.384	8.069	141.90	141.91	-1.613	-1.613	-1.796
$^{212}_{84}\text{Po}$	22	8.882	8.954	154.55	155.20	-6.928	-6.934	-6.532
$^{212}_{86}\text{Rn}$	20	8.462	6.385	140.91	141.43	2.694	2.687	3.155
$^{212}_{88}\text{Th}$	20	3.204	7.958	141.27	141.22	-1.295	-1.294	-1.499
$^{214}_{84}\text{Po}$	22	7.048	7.834	155.32	155.30	-4.058	-4.058	-3.788
$^{214}_{86}\text{Rn}$	22	6.681	9.208	154.63	155.63	-6.797	-6.808	-6.587
$^{214}_{88}\text{Ra}$	20	6.364	7.273	140.21	140.58	0.140	0.136	0.387
$^{214}_{90}\text{Th}$	20	4.116	7.827	140.70	140.51	-0.896	-0.894	-1.060
$^{216}_{84}\text{Po}$	22	5.417	6.906	155.90	155.44	-1.164	-1.159	-0.842

Table 4: (Continued)

α emitter	G	E_{sh} [MeV]	Q_α [MeV]	V_0^{BSQC} [MeV]	V_0^{Fit} [MeV]	$\log T_{1/2}^{\text{BSQC}}$	$\log T_{1/2}^{\text{Fit}}$	$\log T_{1/2}^{\text{Exp}}$
$^{216}_{86}\text{Rn}$	22	5.260	8.198	155.23	155.70	-4.297	-4.302	-4.538
$^{216}_{88}\text{Ra}$	22	4.817	9.526	154.63	155.97	-6.808	-6.800	-6.764
$^{216}_{90}\text{Th}$	20	4.654	8.072	139.52	139.74	-1.673	-1.676	-1.580
$^{216}_{92}\text{U}$	20	2.948	8.531	140.14	139.69	-2.255	-2.249	-2.161
$^{218}_{84}\text{Po}$	22	4.015	6.115	156.18	155.59	1.865	1.871	2.270
$^{218}_{86}\text{Rn}$	22	4.010	7.262	155.73	155.78	-1.496	-1.496	-1.472
$^{218}_{88}\text{Ra}$	22	3.681	8.540	155.19	156.02	-4.452	-4.461	-4.524
$^{218}_{90}\text{Th}$	22	3.317	9.849	154.51	156.21	-6.811	-6.831	-6.914
$^{218}_{92}\text{U}$	20	3.342	8.775	139.08	138.89	-2.962	-2.960	-3.451
$^{220}_{86}\text{Rn}$	22	2.885	6.405	156.11	155.88	1.632	1.636	1.745
$^{220}_{88}\text{Ra}$	22	2.874	7.594	155.70	156.01	-1.735	-1.739	-1.742
$^{220}_{90}\text{Th}$	22	2.331	8.973	154.94	156.27	-4.779	-4.818	-4.991
$^{222}_{86}\text{Rn}$	22	1.933	5.590	156.44	155.97	5.284	5.259	5.519
$^{222}_{88}\text{Ra}$	22	2.201	6.678	156.17	155.99	1.463	1.465	1.526
$^{222}_{90}\text{Th}$	22	1.745	8.133	155.40	156.23	-2.571	-2.581	-2.650
$^{222}_{92}\text{U}$	22	1.263	9.481	154.65	156.42	-5.320	-5.338	-5.328
$^{224}_{88}\text{Ra}$	22	1.617	5.789	156.59	155.95	5.309	5.318	5.497
$^{224}_{90}\text{Th}$	22	1.430	7.299	155.75	156.13	0.063	0.059	0.017
$^{224}_{92}\text{U}$	22	0.826	8.628	155.04	156.36	-3.184	-3.199	-3.402
$^{226}_{88}\text{Ra}$	22	1.259	4.871	157.06	155.83	10.395	10.461	10.703
$^{226}_{90}\text{Th}$	22	1.276	6.453	156.12	155.96	3.274	3.276	3.265
$^{226}_{92}\text{U}$	22	0.842	7.701	155.54	156.16	-0.432	-0.442	-0.570
$^{228}_{90}\text{Th}$	22	1.308	5.520	156.61	155.69	7.685	7.695	7.781
$^{228}_{92}\text{U}$	22	1.138	6.800	156.07	155.85	2.856	2.778	2.748
$^{230}_{90}\text{Th}$	22	1.345	4.770	156.86	155.40	12.167	12.183	12.377
$^{230}_{92}\text{U}$	22	1.462	5.992	156.43	155.47	6.293	6.305	6.243
$^{230}_{94}\text{Pu}$	22	1.097	7.178	155.92	155.69	2.217	2.220	2.021
$^{232}_{90}\text{Th}$	22	1.409	4.082	157.02	155.04	17.358	17.381	17.645
$^{232}_{92}\text{U}$	22	1.746	5.414	156.34	155.08	9.324	9.315	9.336
$^{232}_{94}\text{Pu}$	22	1.545	6.716	155.77	155.29	4.013	4.019	4.004
$^{234}_{92}\text{U}$	22	2.010	4.858	156.33	154.63	12.714	12.719	12.889
$^{234}_{94}\text{Pu}$	22	1.972	6.310	155.57	154.86	5.755	5.763	5.723
$^{234}_{96}\text{Cm}$	22	1.776	7.365	155.35	155.03	2.363	2.367	2.286
$^{236}_{92}\text{U}$	22	2.042	4.573	155.96	154.31	14.675	14.695	14.869
$^{236}_{94}\text{Pu}$	22	2.375	5.867	155.42	154.39	7.872	7.883	7.955
$^{236}_{96}\text{Cm}$	22	2.216	7.067	154.90	154.61	3.485	3.490	3.356
$^{238}_{92}\text{U}$	22	2.003	4.270	155.63	154.00	16.990	17.009	17.149
$^{238}_{94}\text{Pu}$	22	2.611	5.593	154.95	153.98	9.318	9.308	9.442
$^{238}_{96}\text{Cm}$	22	2.746	6.670	154.69	154.10	5.082	5.089	5.314
$^{238}_{98}\text{Cf}$	22	1.966	8.130	153.92	154.54	0.547	0.540	-0.074
$^{240}_{94}\text{Pu}$	22	2.629	5.256	154.66	153.63	11.231	11.245	11.316
$^{240}_{96}\text{Cm}$	22	3.127	6.398	154.32	153.63	6.262	6.270	6.420
$^{240}_{98}\text{Cf}$	22	2.853	7.711	153.65	153.93	1.961	1.947	1.612
$^{242}_{94}\text{Pu}$	22	2.546	4.984	154.31	153.32	12.915	12.927	13.072
$^{242}_{96}\text{Cm}$	22	3.209	6.216	153.85	153.28	7.084	7.091	7.149
$^{242}_{98}\text{Cf}$	22	3.289	7.517	153.18	153.46	2.604	2.600	2.535
$^{244}_{94}\text{Pu}$	22	2.461	4.666	154.03	152.98	15.089	15.102	15.410
$^{244}_{96}\text{Cm}$	22	3.257	5.902	153.45	152.89	8.634	8.644	8.757
$^{244}_{98}\text{Cf}$	22	3.541	7.329	152.72	153.04	3.273	3.269	3.193
$^{244}_{98}\text{Fm}$	22	2.966	8.550	152.19	153.40	0.073	-0.017	-0.506
$^{246}_{96}\text{Cm}$	22	3.273	5.475	153.31	152.45	10.946	10.957	11.173
$^{246}_{98}\text{Cf}$	22	3.801	6.862	152.64	152.54	5.108	5.109	5.111

Table 4: (Continued)

α emitter	G	E_{sh} [MeV]	Q_α [MeV]	V_0^{BSQC} [MeV]	V_0^{Fit} [MeV]	$\log T_{1/2}^{\text{BSQC}}$	$\log T_{1/2}^{\text{Fit}}$	$\log T_{1/2}^{\text{Exp}}$
^{246}Fm	22	3.590	8.379	151.68	152.86	0.492	0.478	0.217
^{100}Cm	22	3.159	5.162	153.03	152.09	12.824	12.835	13.079
^{248}Cf	22	4.024	6.361	152.62	152.00	7.307	7.315	7.459
^{248}Fm	22	3.923	7.995	151.50	152.36	1.716	1.706	1.538
^{250}Cf	22	3.986	6.129	152.13	151.61	8.422	8.430	8.616
^{250}Fm	22	4.335	7.557	151.39	151.79	3.233	3.228	3.270
^{252}Cf	22	3.459	6.217	151.33	151.52	7.949	7.947	7.935
^{252}Fm	22	4.655	7.154	151.26	151.21	4.757	4.757	4.961
^{252}No	22	4.374	8.549	150.46	151.59	0.703	0.689	0.562
^{102}Cf	22	2.996	5.927	151.05	151.30	9.389	9.386	9.228
^{254}Fm	22	4.147	7.307	150.27	151.09	4.131	4.121	4.068
^{102}No	22	4.809	8.226	150.21	151.00	1.707	1.698	1.755
^{100}Fm	22	3.618	7.025	149.98	150.86	5.231	5.220	5.064
^{256}No	22	4.478	8.582	148.98	150.81	0.564	0.538	0.466
^{256}Rf	22	5.029	8.926	149.78	150.65	0.299	0.308	0.328
^{258}Rf	22	4.912	9.196	148.65	150.35	-0.497	-0.517	-0.593
^{260}Sg	22	5.331	9.901	148.13	149.89	-1.628	-1.678	-1.767
^{106}Hs	22	5.394	10.346	146.66	148.61	-2.116	-2.144	-2.403
^{108}Hs	22	6.391	9.070	147.10	147.05	1.276	1.277	0.954
^{110}Ds	22	5.365	11.117	145.44	147.77	-3.246	-3.293	-3.688
^{286}Fl	22	6.502	10.355	143.83	142.84	-0.166	-0.252	-0.657
^{114}Fl	22	6.731	10.076	143.53	142.08	0.454	0.487	-0.185
^{294}Og	22	7.380	11.867	141.63	140.26	-2.550	-2.533	-3.155

is $a_0 = 0.64$ fm, yielding an rms deviation of $\chi_{\text{Fit}} = 0.251$, which is slightly smaller than the value $\chi_{\text{DF}} = 0.259$ obtained using the DF approach. A regional analysis for nuclei sharing the same global quantum number G , also shown in Figure 3, reveals that the $G = 20$ group exhibits noticeably larger deviations than the $G = 18$ and $G = 22$ regions. This behavior is consistent with the stronger fluctuations of the logarithmic errors $\log(T_{1/2}^{\text{Cal}}/T_{1/2}^{\text{Exp}})$ around zero observed in Figure 2.

The sensitivity to the radius parameter r_0 is illustrated in Figure 4, where the rms deviation χ is shown as a function of r_0 with the diffuseness fixed at $a_0 = 0.64$ fm. Compared to the diffuseness, the dependence on r_0 is smoother and less pronounced. Variations of r_0 primarily lead to a uniform rescaling of the potential geometry, which can be partially compensated by corresponding adjustments of the potential depth V_0 . The optimal value $r_0 = 1.27$ fm adopted in this work is therefore determined from a global minimization of χ for the full set of 178 nuclei, providing a consistent and robust choice for systematic α -decay calculations.

4. Conclusion

In this work, α -decay half-lives of 178 even-even nuclei have been calculated within the semi-classical WKB framework using a phenomenological WS potential. The novelty of the present work lies not in proposing a new decay model, but in establishing a physically constrained and computationally efficient framework that bridges direct BSQC-based calculations

and global phenomenological parametrizations. When the potential depth V_0 is determined directly from the BSQC, an rms deviation of $\chi_{\text{BSQC}} = 0.253$ is obtained, confirming the reliability of the WS potential constrained by semi-classical quantization for systematic α -decay calculations.

Based on the BSQC-determined depths, a fitted parametrization of the WS potential depth has been constructed. The resulting half-lives yield a comparable rms deviation of $\chi_{\text{Fit}} = 0.250$, demonstrating that the fitted prescription preserves the accuracy of the direct BSQC approach. From a practical perspective, this parametrization significantly reduces the computational cost by avoiding repeated semi-classical integral evaluations, while maintaining consistency and reliability in large-scale calculations.

The present study focuses on even-even nuclei, where α decay predominantly occurs between ground states and angular-momentum hindrance effects are minimal. In this sense, the proposed approach should be regarded as a first step toward a global and efficient description of α decay based on phenomenological potentials constrained by semi-classical quantization. Extensions to odd- A and odd-odd nuclei, as well as the inclusion of additional structural effects such as deformation and explicit preformation dynamics [34–38], will be addressed in future work.

Overall, the fitted WS potential depth provides an efficient and accurate tool for systematic α -decay studies, offering a practical framework for applications to heavy and superheavy nuclei.

Acknowledgements

The authors thank Le Hoang Chien (VNU-HCMUS) and Bui Minh Loc (SDSU) for providing numerical data and for valuable discussions in this work. This research is funded by the Vietnam National Foundation for Science and Technology Development (NAFOSTED) under grant number 103.04-2025.07.

References

- [1] C. Qi, R. Liotta, R. Wyss, Recent developments in radioactive charged-particle emissions and related phenomena, *Prog. Part. Nucl. Phys.* 105 (2019) 214–251. [doi:10.1016/j.ppnp.2018.11.003](https://doi.org/10.1016/j.ppnp.2018.11.003).
- [2] M. Pfützner, M. Karny, L. V. Grigorenko, K. Riisager, Radioactive decays at limits of nuclear stability, *Rev. Mod. Phys.* 84 (2012) 567–619. [doi:10.1103/RevModPhys.84.567](https://doi.org/10.1103/RevModPhys.84.567).
- [3] C. Xu, Z. Ren, Global calculation of α -decay half-lives with a deformed density-dependent cluster model, *Phys. Rev. C* 74 (2006) 014304. [doi:10.1103/PhysRevC.74.014304](https://doi.org/10.1103/PhysRevC.74.014304).
- [4] J.-G. Deng, H.-F. Zhang, Correlation between α -particle preformation factor and α decay energy, *Phys. Lett. B* 816 (2021) 136247. [doi:10.1016/j.physletb.2021.136247](https://doi.org/10.1016/j.physletb.2021.136247).
- [5] H. F. Zhang, G. Royer, α particle preformation in heavy nuclei and penetration probability, *Phys. Rev. C* 77 (2008) 054318. [doi:10.1103/PhysRevC.77.054318](https://doi.org/10.1103/PhysRevC.77.054318).
- [6] W. Zhang, Y. Gao, J. Cui, Y. Wang, J. Gu, Roles of spin-orbit interaction and pairing correlation in α decay of ^{210}Po , *Phys. Rev. C* 112 (2025) 024319. [doi:10.1103/dw7k-fj9j](https://doi.org/10.1103/dw7k-fj9j).
- [7] J.-G. Deng, H.-F. Zhang, Analytic formula for estimating the α -particle preformation factor, *Phys. Rev. C* 102 (2020) 044314. [doi:10.1103/PhysRevC.102.044314](https://doi.org/10.1103/PhysRevC.102.044314).
- [8] D. Ni, Z. Ren, Microscopic calculation of α -decay half-lives within the cluster model, *Nucl. Phys. A* 825 (3) (2009) 145–158. [doi:10.1016/j.nuclphysa.2009.04.010](https://doi.org/10.1016/j.nuclphysa.2009.04.010).
- [9] X.-D. Sun, P. Guo, X.-H. Li, Systematic study of α decay half-lives for even-even nuclei within a two-potential approach, *Phys. Rev. C* 93 (2016) 034316. [doi:10.1103/PhysRevC.93.034316](https://doi.org/10.1103/PhysRevC.93.034316).
- [10] D. S. Delion, Theory of particle and cluster emission, Vol. 819, Springer, 2010.
- [11] W. Yong-Jia, Z. Hong-Fei, Z. Wei, L. Jun-Qing, Improvement of a fission-like model for nuclear α decay, *Chinese Phys. Lett.* 27 (6) (2010) 062103. [doi:10.1088/0256-307X/27/6/062103](https://doi.org/10.1088/0256-307X/27/6/062103).
- [12] G. Gamow, Zur quantentheorie des atomkernes, *Z. Phys.* 51 (3) (1928) 204–212. [doi:10.1007/BF01343196](https://doi.org/10.1007/BF01343196).
- [13] R. W. Gurney, E. U. Condon, Wave mechanics and radioactive disintegration, *Nature* 122 (3073) (1928) 439–439. [doi:10.1038/122439a0](https://doi.org/10.1038/122439a0).
- [14] R. W. Gurney, E. U. Condon, Quantum Mechanics and Radioactive Disintegration, *Phys. Rev.* 33 (1929) 127–140. [doi:10.1103/PhysRev.33.127](https://doi.org/10.1103/PhysRev.33.127).
- [15] N. G. Kelkar, H. M. Castañeda, Critical view of WKB decay widths, *Phys. Rev. C* 76 (2007) 064605. [doi:10.1103/PhysRevC.76.064605](https://doi.org/10.1103/PhysRevC.76.064605).
- [16] L. H. Chien, N. T. T. Phuc, On the Bohr-Sommerfeld quantization condition and assault frequency in a semi-classical model for α decay, *Nucl. Phys. A* 1018 (2022) 122373. [doi:10.1016/j.nuclphysa.2021.122373](https://doi.org/10.1016/j.nuclphysa.2021.122373).
- [17] N. N. Le, Implications of repulsive core effects in double-folding potentials for α decay of heavy and superheavy nuclei, *Nucl. Phys. A* 1063 (2025) 123217. [doi:10.1016/j.nuclphysa.2025.123217](https://doi.org/10.1016/j.nuclphysa.2025.123217).
- [18] M. Lu, N. Wan, Effects of different effective nucleon-nucleon interactions on α -decay half-life and extracted α -cluster preformation probability, *Phys. Rev. C* 110 (2024) 044321. [doi:10.1103/PhysRevC.110.044321](https://doi.org/10.1103/PhysRevC.110.044321).
- [19] D. Ni, Z. Ren, α -Decay calculations of medium mass nuclei within generalized density-dependent cluster model, *Nucl. Phys. A* 828 (3-4) (2009) 348–359. [doi:10.1016/j.nuclphysa.2009.07.014](https://doi.org/10.1016/j.nuclphysa.2009.07.014).
- [20] C. Xu, Z. Ren, Favored α -decays of medium mass nuclei in density-dependent cluster model, *Nucl. Phys. A* 760 (3) (2005) 303–316. [doi:10.1016/j.nuclphysa.2005.06.011](https://doi.org/10.1016/j.nuclphysa.2005.06.011).
- [21] Y. Qian, Z. Ren, D. Ni, Calculations of α -decay half-lives for heavy and superheavy nuclei, *Phys. Rev. C* 83 (2011) 044317. [doi:10.1103/PhysRevC.83.044317](https://doi.org/10.1103/PhysRevC.83.044317).
- [22] E. Shin, Y. Lim, C. H. Hyun, Y. Oh, Nuclear isospin asymmetry in α decay of heavy nuclei, *Phys. Rev. C* 94 (2016) 024320. [doi:10.1103/PhysRevC.94.024320](https://doi.org/10.1103/PhysRevC.94.024320).
- [23] J. Tian, K. Ren, P. Ma, C. Li, N. Wang, Shell correction dependence of potential depth in an α -decay cluster model, *Phys. Rev. C* 110 (2024) 064313. [doi:10.1103/PhysRevC.110.064313](https://doi.org/10.1103/PhysRevC.110.064313).
- [24] B. Buck, A. Merchant, S. Perez, Half-Lives of Favored Alpha Decays from Nuclear Ground States, *At. Data Nucl. Data Tables* 54 (1) (1993) 53–73. [doi:10.1006/adnd.1993.1009](https://doi.org/10.1006/adnd.1993.1009).
- [25] X. Bao, H. Zhang, H. Zhang, G. Royer, J. Li, Systematical calculation of α decay half-lives with a generalized liquid drop model, *Nucl. Phys. A* 921 (2014) 85–95. [doi:10.1016/j.nuclphysa.2013.11.002](https://doi.org/10.1016/j.nuclphysa.2013.11.002).

[26] M. Wang, W. J. Huang, F. G. Kondev, G. Audi, S. Naimi, The AME 2020 atomic mass evaluation (II). Tables, graphs and references, Chin. Phys. C 45 (3) (2021) 030003. [doi:10.1088/1674-1137/abddaf](https://doi.org/10.1088/1674-1137/abddaf).

[27] B. Buck, J. C. Johnston, A. C. Merchant, S. M. Perez, Cluster model of α decay and ^{212}Po , Phys. Rev. C 53 (1996) 2841–2848. [doi:10.1103/PhysRevC.53.2841](https://doi.org/10.1103/PhysRevC.53.2841).

[28] K. Wildermuth, Y. Tang, A unified theory of the nucleus, Springer-Verlag, 1977. [doi:10.1007/978-3-322-85255-7](https://doi.org/10.1007/978-3-322-85255-7).

[29] R. E. Langer, On the Connection Formulas and the Solutions of the Wave Equation, Phys. Rev. 51 (1937) 669–676. [doi:10.1103/PhysRev.51.669](https://doi.org/10.1103/PhysRev.51.669).

[30] J. J. Morehead, Asymptotics of radial wave equations, Journal of Mathematical Physics 36 (10) (1995) 5431–5452. [doi:10.1063/1.531270](https://doi.org/10.1063/1.531270).

[31] F. Kondev, M. Wang, W. Huang, S. Naimi, G. Audi, The NUBASE2020 evaluation of nuclear physics properties, Chin. Phys. C 45 (3) (2021) 030001. [doi:10.1088/1674-1137/abddae](https://doi.org/10.1088/1674-1137/abddae).

[32] K. Varga, R. G. Lovas, R. J. Liotta, Absolute alpha decay width of ^{212}Po in a combined shell and cluster model, Phys. Rev. Lett. 69 (1992) 37–40. [doi:10.1103/PhysRevLett.69.37](https://doi.org/10.1103/PhysRevLett.69.37).

[33] K. Varga, R. G. Lovas, R. J. Liotta, Cluster-configuration shell model for alpha decay, Nucl. Phys. A 550 (3) (1992) 421–452. [doi:10.1016/0375-9474\(92\)90017-E](https://doi.org/10.1016/0375-9474(92)90017-E).

[34] D. Deng, Z. Ren, α preformation factors of medium-mass nuclei and the structural effects in the region of crossing the $Z = 82$ shell, Phys. Rev. C 93 (2016) 044326. [doi:10.1103/PhysRevC.93.044326](https://doi.org/10.1103/PhysRevC.93.044326).

[35] X.-D. Sun, C. Duan, J.-G. Deng, P. Guo, X.-H. Li, Systematic study of α decay for odd- A nuclei within a two-potential approach, Phys. Rev. C 95 (2017) 014319. [doi:10.1103/PhysRevC.95.014319](https://doi.org/10.1103/PhysRevC.95.014319).

[36] X. Sun, Y. Cui, F. Zou, K. Xing, J. Tian, N. Wang, Nuclear α decay based on the pick-up mechanism, Phys. Rev. C 111 (2025) 064319. [doi:10.1103/ryvc-5r6x](https://doi.org/10.1103/ryvc-5r6x).

[37] V. Y. Denisov, Empirical relations for α -decay half-lives: The effect of deformation of daughter nuclei, Phys. Rev. C 110 (2024) 014604. [doi:10.1103/PhysRevC.110.014604](https://doi.org/10.1103/PhysRevC.110.014604).

[38] H. Zheng, D. Deng, Z. Ren, Effect of deformation on α clustering from a pocket-type dynamical double-folding potential, Phys. Rev. C 112 (2025) 064320. [doi:10.1103/hqtq-xvyp](https://doi.org/10.1103/hqtq-xvyp).